
ANISOTROPIC MAGNETOTRANSPORT REALIZED IN DOPED HEMATITE

A PREPRINT

✉ E.F. Galindez-Ruales¹, L. Šmejkal^{1,2}, S. Das¹, E. Baek^{1,3}, ✉ C. Schmitt¹, ✉ F. Fuhrmann¹, ✉ A. Ross¹,
R. González-Hernández^{1,4}, A. Rothschild⁵, J. Sinova¹, C.-Y. You³, ✉ G. Jakob¹, ✉ M. Kläui^{1,6*}

1 Institute of Physics, Johannes Gutenberg University Mainz, Staudingerweg 7, 55128 Mainz, Germany.

2 Institute of Physics, Academy of Sciences of the Czech Republic, 182 00 Prague 8, Czech Republic.

3 Department of Physics and Chemistry, DGIST, Daegu 42988, Republic of Korea.

4 Grupo de Investigación en Física Aplicada, Departamento de Física, Universidad del Norte, Barranquilla, Colombia.

5 Department of Materials Science and Engineering, Technion-Israel Institute of Technology, Haifa 32000, Israel.

6 Center for Quantum Spintronics, Norwegian University of Science and Technology, Trondheim 7491, Norway.

* klaeui@uni-mainz.de

October 27, 2023

ABSTRACT

Conventional antiferromagnetic materials have long been recognized for their time-reversal symmetry, resulting in a zero anomalous Hall coefficient. However, a paradigm shift occurs when examining easy-axis antiferromagnets and their spin-flop transition. This transition introduces a magnetic canted moment, leading to the emergence of a non-zero anomalous Hall signal and the generation of a non-dissipative transversal current. While high symmetry systems typically manifest an isotropic Hall effect, our study unveils the extraordinary behavior exhibited by hematite that becomes conductive due to small Ti doping. We investigate the magnetotransport in Titanium-doped hematite, uncovering a highly pronounced and unconventional symmetry. Notably, this effect displays a remarkable dependence on the crystal orientation of the material. We establish a compelling correlation between our experimental observations and the predicted anomalous Hall effect in altermagnets through symmetry analysis. This study expands our understanding of the Hall effect in antiferromagnetic materials and sheds light on the intricate interplay between crystal orientation and unconventional Hall phenomena.

Keywords Magneto transport · Hall effect · anisotropy · hematite · antiferromagnets · altermagnets · spin-flop transition

Introduction

Hematite (α -Fe₂O₃) is a widely studied material in the field of solid-state physics due to its rich electronic and magnetic properties. It has garnered significant attention in recent years, particularly in the realm of spintronics and other emerging applications [1–9]. The antiferromagnetic structure of hematite has been extensively investigated, primarily focusing on its relationship to spin transport based on magnons [5]. At temperatures between 265 and 960 K, hematite exhibits weak ferromagnetism, with the antiferromagnetically ordered spins slightly tilted in the basal plane. However, below the Morin transition (MT) temperature of 265 K, the spins reorient to align parallel to the c-axis, forming a collinear antiferromagnetic magnetic order. This transition is attributed to the delicate balance between magnetic-dipole and single-ion anisotropy energies [10]. These two distinct states, referred to as the weak ferromagnetic (WFM) and collinear antiferromagnetic (AFM) states, respectively, have been extensively investigated [11]. To tune the properties of hematite, doping has been used [12, 13]. In particular, it was found that the introduction of low percentages of certain dopants can induce changes in anisotropies and shift the Morin transition temperature while having minimal impact on the overall magnetic properties, such as the magnitude of the magnetic moment [13] and the presence of the Morin transition (MT) [5, 14]. Additionally, hematite films may exhibit altered Morin transition behavior due to growth-induced strain, which can modify lattice constants and anisotropies [5].

In addition to these magnetic properties, reports in the literature have discussed the observation of the Hall effect in doped hematite that can become electrically conducting. Anomalous-like Hall behavior, similar to that typically seen in ferromagnets when a magnetic field is applied along the c-axis, has been observed in hematite [12, 15]. However, in many experimental investigations, the resistivity of the samples has been too high, resulting in a zero Hall coefficient when the field was oriented along the c-axis [16, 17]. Nonetheless, heavily doped samples have exhibited more conventional Hall effect behavior, with the Hall voltage being directly proportional to the applied field within a temperature range of 190 to 290 K [18]. Several materials have shown new Hall effects based on magnetic properties, such as the Spin Hall effect, inverse Spin Hall effect, or quantum spin Hall effect, among others [19].

Recently, novel transport effects have been predicted in systems with particular symmetry. Hematite is considered to belong to the class of altermagnets [20–22] however, work is still required to ascertain the altermagnetic properties. The Anomalous Hall Effect (AHE), initially studied in ferromagnetic materials, has gained importance in the investigation of antiferromagnets (AFMs) [23, 24]. It is known that the AHE can occur in noncoplanar antiferromagnets even without the presence of spin-orbit interaction. Altermagnets have properties similar to AFMs, so similar methods could be exploited. In collinear antiferromagnets, the AHE can arise due to the induced canted moment during spin reorientation, breaking the symmetry and resulting in a non-zero AHE. Furthermore, the structural order of non-magnetic atoms and their chirality can also contribute to the origin of the induced moment and the AHE [22, 25, 26].

Given these intriguing observations, a key open question is the origin and symmetry of the magnetotransport in hematite and the understanding of the mechanisms. Specifically, elucidating the contribution from the Anomalous Hall Effect (AHE) and its origin. So far, either the induced magnetization on the spin reorientation or from some hidden mechanism from its altermagnetic nature. Experimentally, so far, the origin could not be determined as the AHE has only been probed in simple geometries without the necessary angular dependence to allow for the required symmetry analysis. So, one could not relate the experimental results to the predicted AHE in altermagnets is attributed exclusively to the crystal structure [22]. The non-zero AHE coefficient there comes from the presence of non-magnetic atoms at noncentrosymmetric positions, despite the inversion center at the magnetic atoms. However, measuring a Hall voltage on hematite presents challenges due to its insulating nature. Doping the material becomes necessary to overcome this limitation and access the transport properties. It is crucial to carefully select magnetic and non-magnetic dopants to avoid inducing stress and altering the properties of hematite [12, 13, 27]. Based on previous reports [15, 28], it has been concluded that when the doping level is below 2%, the dopants added to the material will be fully ionized at all our temperatures. Consequently, the number of carriers present in the material is expected to remain relatively constant with temperature, changing by no more than one order of magnitude, and the low doping level does not significantly affect the magnetism.

In this article, we ascertain the anisotropic anomalous Hall effect in hematite with low Ti doping. This material possesses the necessary crystal structure and magnetic ordering symmetries that can lead to generating a transverse voltage when particular symmetries are broken. By introducing low doping levels, we effectively close the bandgap by putting defect states into the energy gap, enabling access to the electronic transport properties of the material. Specifically, we study 1% Ti-doped hematite thin films with a thickness of 150 nm, highlighting the intriguing characteristics of the anomalous Hall effect in this system. Our measurements reveal a strong anisotropy in the crystal orientation dependence of the Hall effect, demonstrating a pronounced sensitivity to the crystallographic axis. We observe a sign inversion in the antisymmetric part of the signal, which defies intuitive expectations. This investigation reveals novel symmetry-related properties of hematite's electronic and magnetic properties. In particular, we discover an unconventional crystal dependence of the transverse voltage and an unintuitive sign inversion in the antisymmetric part that is elucidated by high-precision angular-dependent Hall measurements.

Results and discussion

The discovery of altermagnets suggests a new classification of magnetic materials that exhibit fascinating characteristics beyond those of traditional antiferromagnets [29]. These altermagnetic materials, such as ruthenium oxide, hematite, and various other compounds, display intriguing traits such as spin splitting and non-zero anomalous Hall coefficients [29]. Hematite, as an example of an altermagnetic material, potentially exhibits these unique properties. Its hexagonal crystalline structure (Fig. 1.a) consists of two sub-lattices of iron atoms with oxygen atoms positioned at non-centrosymmetric sites. At different temperatures, hematite exhibits three distinct non-paramagnetic phases, as illustrated in Fig. 1.b, which can be described using magnetic space and point groups. By controlling the percentage of material

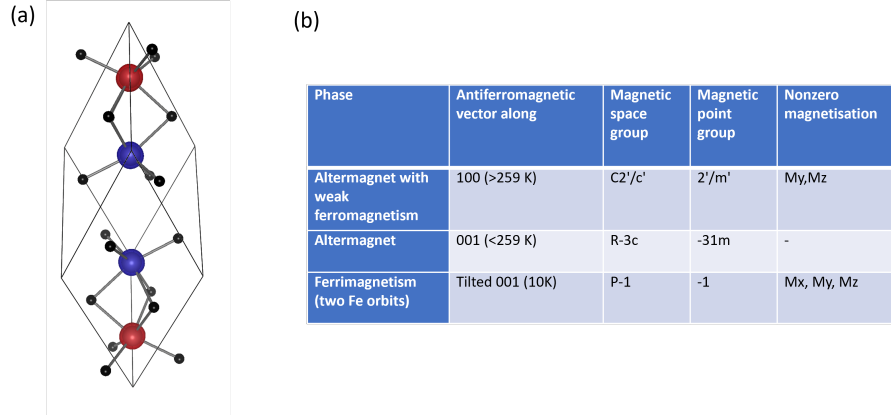


Figure 1: (a) Visual representation of hematite's hexagonal crystal structure, showcasing the two iron sublattices (red and blue) and the oxygen atoms (black) in non-centrosymmetric positions. (b) The different magnetic phases of hematite, with corresponding magnetic space and point groups. The Morin temperature defines the altermagnetic phases that have and lack weak ferromagnetism, resulting in a non-zero magnetization at high temperatures.

doping, in our case, we can shift the Fermi level by some tenths of eV [30, 31], providing access to the electronic transport properties of the material while keeping the antiferromagnetic properties of hematite.

High-quality 150 nm films of 1% Ti-doped hematite were fabricated (refer to the Materials and Methods section for detailed fabrication procedures). Hall bars were patterned at various in-plane orientations relative to the \mathbf{a} -axis. Magnetization measurements (Fig. 2.b) revealed a decrease in the magnetic moment below 338 K, which was identified as the Morin transition (MT). Unlike a single crystal sample [10], this transition exhibits a broader nature, attributed to the existence of a multidomain state in our samples [5]. The easy-axis phase (shown in Figure 2.a) does not exhibit a significant magnetic moment as expected for a system with magnetic properties of hematite. Furthermore, the magnitude of the canted moment agrees with the bulk value, as reported in references [4] and [11]. The absence of secondary phases (see Supporting Information), highly epitaxial thin films, well-defined in-plane orientation, the presence of the Morin transition, and the lack of a higher canted magnetic moment suggest that the doping level does not significantly impact the magnetic properties of hematite. Determining the conducting regime is essential in selecting the appropriate analysis approach. In the case of our poorly conducting samples, this is achieved by studying the resistivity behavior as a function of temperature (blue line in Fig. 2.c). While a semiconductor-like model fits reasonably well, the slope yields a gap of $1600 k_B$, which does not align with the gap of hematite. Moreover, the thermal activation factor value (5×10^{-3}) suggests that the transport mechanism is likely variable-range hopping [32].

Given the percentage of dopants in our samples (1%), we expect a relatively large number of charge carriers (approximately 10^{15} cm^{-3} in our case). Thus, conduction via hopping in the impurity "band" of the donors would be most probable. The relatively low doping level allows for the measurement of some Hall conductivity in the poorly conducting regime [33], without significantly altering the intriguing symmetry properties of hematite. This is evident in the very low conventional Hall coefficient (approximately $5 \text{ cm}^3 \text{ C}^{-1}$) observed over a wide range of temperatures (Figure 3) [18, 28]. However, the anomalous Hall signal increases around the spin flop transition (Fig. 3.a).

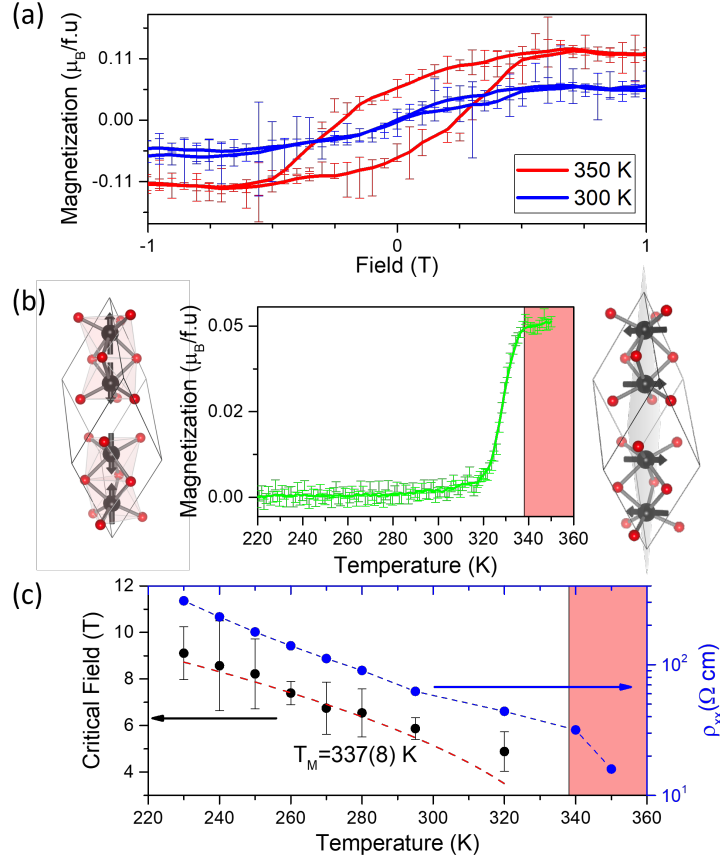


Figure 2: Measurements of SQUID magnetometry for a magnetic field applied perpendicular to the c -axis. (a) Magnetization per formula unit as a function of the field for the Ti-doped samples in both the collinear phase (300 K) and the weak ferromagnetic phase (350 K). At high temperatures, the hysteresis loop for the canted moment saturates at 0.5 T. The signal observed at lower temperatures is attributed to the nucleation of the γ - Fe_2O_3 phase at the substrate interface. (b) The magnetization as a function of temperature under an external magnetic field of 20 mT reveals a decrease in magnetization as temperature increases due to the Morin transition. This transition from the collinear phase (left panel) to the weak ferromagnetic phase (right panel) occurs over a temperature range of 20 Kelvin. (c) The critical field (H_c) required to reach the spin flop state varies depending on the temperature, as well as the longitudinal resistivity decreases proportionally. H_c is well described by $H_{cr}(T) \propto \sqrt{T_M - T}$ following the Landau theory, while the resistivity behaves as transport due to hopping in the impurity band of the donors.

The Hall signal in the collinear phase is almost zero at low fields, followed by a substantial anomalous behavior around the spin-flop transition. At the spin-flop transition, the Néel vector undergoes a rotation from the out-of-plane (OOP) direction into the basal plane, resulting in a canted magnetic moment. The critical field is determined where the transverse resistivity increases, and it is energy-equivalent to the Morin transition. The temperature dependence of the critical field is well described by $H_{cr} \propto \sqrt{T_M - T}$ (red dotted line in Fig 2.c), with a critical temperature (T_M) of $337 \pm 8 \text{ K}$. This behavior aligns with a typical second-order phase transition within the Landau theory, as previously reported [34, 35]. However, the presence of a multidomain state in our sample leads to a different definition of the Morin transition compared to this critical temperature. In our case, the critical point is determined as the point where the slope starts changing, either when decreasing the temperature (MT) or increasing the field (H_c).

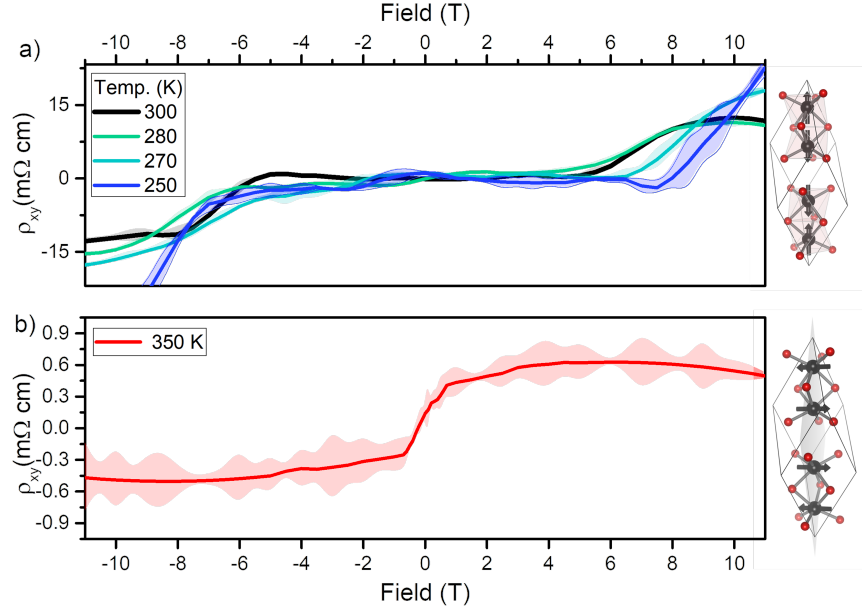


Figure 3: Hall resistivity in relation to the OOP field for temperatures below (a) and above (b) the Morin transition. The shifting of the critical field with temperature in the collinear phase indicates the equivalence between the spin-flop and the Morin transition as expected for hematite. On the right side of the graph, the magnetic configurations of the Fe atoms in both phases are displayed while maintaining crystal symmetries.

In the collinear phase (Fig 3.a), when an out-of-plane (OOP) field is applied, a fully antisymmetric signal is observed only when the current direction is parallel to one of the three **a**-axes. A small hysteretic behavior in the Hall signal may be attributed to possible magnetic domain configurations [5, 13]. The size of the domains present in each structure can differ due to strain-induced anisotropy introduced during the patterning process [36].

In the weak ferromagnetic phase (Fig 3.b), the Hall signal agrees with the expected behavior from the Anomalous Hall Effect (AHE), as it saturates in accordance with the canted moment of the samples.

Interesting behavior arises when the Hall bar is patterned in an orientation that deviates from the high symmetry **a**-axis (Fig. 4). When the current channel is along a lower symmetry axis, it allows access to the symmetric components of the conductivity tensor (Fig. 4.b). This effect is only observed when the conductivity components are anisotropic and the orientation of the Hall bar is appropriate. This effect is zero in highly symmetric orientations (black and gray lines), while in less symmetrical orientations (purple and blue lines), the even part of the conductivity has a larger contribution than the odd part.

The odd part of the Hall conductivity for Hall bars with different orientations relative to the **a**-axis exhibits a sign inversion at 30, 45, and 90 degrees but preserves the sign at rotations of 120 degrees (Figure 4.c). This behavior is unexpected within the framework of conventional hopping transport and suggests that it may be attributed to spin-splitting from the altermagnetic nature. However, we note that in our poorly conducting transport regime, we cannot quantify altermagnetic spin-splitting effects.

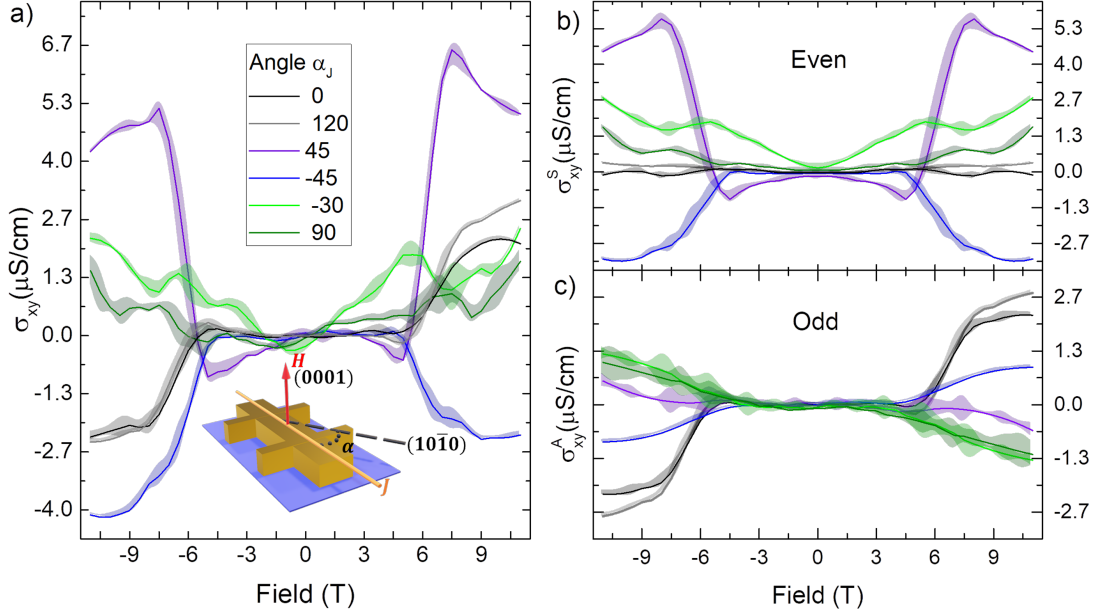


Figure 4: (a) The Hall conductivity at 300 K of different devices measured at various angles relative to the in-plane crystallographic axis, denoted as \mathbf{a} ($10\bar{1}0$). A diagram illustrating the different device orientations is provided below. Following symmetrization (as stated in Eq. 4), the even (b) and odd (c) contributions are distinguished. The even contribution exhibits significantly different weight in the Hall signal across the various relative orientations, whereas the odd portion's sign inversion cannot be attributed to weak moment-induced anomalous Hall effect contribution.

In terms of symmetry, the shift from the \mathbf{a} -axis oriented Hall bar to the $\pm 45^\circ$ orientation results in a change from a predominantly antisymmetric signal to a symmetric behavior, accompanied by a sign inversion. The odd conductivity components display a decrease in amplitude when the Hall bar is oriented along the \mathbf{a} -axis compared to other orientations. However, the crystal equivalent orientations of the Hall bars exhibit similar symmetry behavior (-30 and 90, 45 and -45, 0 and 120 degrees). An inversion of the sign is observed when the current is at 45 and -45 degrees relative to the \mathbf{a} -axis, as well as from 0 and -30, or 0 and 90 degrees, but not between Hall bars oriented 120 degrees relative to each other.

In the poorly conducting regime of our samples, the dominant transport mechanism is variable-range hopping, accompanied by a low Hall mobility of approximately $0.1 \text{ cm}^2\text{V}^{-1}\text{s}^{-1}$. Despite the limited conductivity, we are able to access both the symmetric and antisymmetric components of the conductivity tensor. The symmetries observed in the Hall effect are directly correlated with the Hall bars' relative orientation and the material's crystallographic structure. Significantly, this dependence on orientation is not influenced by the canted moments induced during spin reorientation, as the induced canted moment remains consistent for all device orientations at a fixed field strength. It can be concluded that the conductivity tensor is non-symmetric, and these non-symmetric terms can only be accessed when the symmetry of the system is lowered, i.e., the current vector is not along a high symmetry axis.

In conclusion, the inversion of the sign in the odd part of the Hall conductivity in hematite may originate from the altermagnetic magnetic properties present in the inaccessible but still representative bands of the material. This sign inversion signifies the presence of unique underlying mechanisms governing the anomalous Hall effect (AHE) in this particular material.

These findings highlight the intricate interplay between crystal structure, magnetic properties, and conductivity in our samples. Investigating the anisotropic anomalous Hall effect in hematite provides significant insights into this material's electronic and magnetic properties. By unraveling the complex relationship between symmetry breaking and the resulting Hall signals, we advance our understanding of this phenomenon and its potential applications in various fields. The intricate symmetry of the Hall signal observed is intriguing and will spark further investigations, particularly for different doping levels that go beyond the current work, to fully understand and elucidate the specific mechanisms responsible for the observed symmetries and sign inversion in the Hall conductivity. Our findings contribute to a deeper knowledge of hematite's behavior, laying the groundwork for its utilization in areas such as electronics, energy storage, and data storage.

Furthermore, this study serves as a stepping stone for exploring similar materials with analogous properties and provides valuable insights that contribute to our broader understanding of electronic and magnetic phenomena. Our research establishes a foundation for future investigations into the anomalous Hall effect in altermagnets and its implications for emerging technologies.

Acknowledgments

This work was supported by the Max Planck Graduate Center with the Johannes Gutenberg-Universität Mainz (MPGC). The authors in Mainz acknowledge support from the DFG project number 423441604. All authors from Mainz also acknowledge support from SPIN + X (DFG SFB TRR 173 No. 268565370, projects A01, A03, and B02). M.K. acknowledges support by the Research Council of Norway through its Centers of Excellence funding scheme, project number 262633 "QuSpin." C.-Y.Y. and E.B. acknowledge support from the National Research Foundation of Korea (Grant No. 2021M3F3A2A01037525).

Supporting Information

Materials and Methods

Thin (0001)-oriented hematite films of 150 nm thickness doped with 1% Ti [α -Fe_{1.99}Ti_{0.01}O₃:(Ti) α -Fe₂O₃] were deposited on c-plane (0001) sapphire substrates using pulsed laser deposition (PLD). The deposition was carried out at a set point temperature of 800 °C under an oxygen partial pressure of 10 mTorr. The films were grown from a stoichiometric doped target, and a total of 20,000 pulses were used to achieve the desired thickness of approximately 150 nm, as described in [37]. The crystallographic purity of the thin films was confirmed using X-ray diffraction (XRD).

Also, the in-plane crystallographic orientation of the sample was determined (See Crystalline and epitaxial-quality determination), and Hall bars were patterned in different orientations with respect to the crystallographic direction **a**.

The temperature range for the colinear phase of the hematite films was determined using superconducting quantum interference device (SQUID) magnetometry measurements (See Magnetometry measurements). All structures were fabricated using two electron beam lithography steps. First, a protective resist mask was defined to allow ion-beam etching until the substrate. Then, contacts were implemented using a lift-off technique with a Cr/Au bilayer. Six different orientations were patterned in the samples, with angles of $\phi = 0, 30, 45, 60, 90, 120^\circ$ in the plane, where $\phi = 0$ points along the **a** axis.

The longitudinal resistance of the Hall bar was measured using a high-impedance electrometer while applying a current of $I = 2 \times 10^6$ A/cm². A highly sensitive nanovoltmeter measured the transverse voltage (V_{xy}). Various voltage components, including the voltmeter offset (V_0), thermoelectric voltages (V_S), Nernst effect voltage, and Righi-Leduc voltage, were subtracted using a current symmetrization technique with the current I of the Hall bar. The Hall resistivity (ρ_{xy}^{Hall}) as a function of the external magnetic field H was calculated by multiplying by the geometrical factor of the Hall bar [38]:

$$\rho_{xy}^{Hall} = R_{xy}^{Hall} \cdot t \quad (1)$$

The longitudinal resistivity is given by:

$$\rho_{xx} = \frac{R_{xx} \cdot w \cdot t}{a} \quad (2)$$

In our case, $t = 150$ nm represents the thickness of the sample, $w = 10$ μm is the width of the Hall bar, and $a = 80$ μm is the distance between the two channels of the 6-point Hall bar.

The Hall conductivity can be calculated using the values of ρ_{xx} and ρ_{xy} :

$$\sigma_{xy} = \frac{\rho_{xy}}{\rho_{xx}^2 + \rho_{xy}^2} \quad (3)$$

To analyze the results under symmetry arguments, the transversal conductivity is symmetrized/anti-symmetrized with respect to the external magnetic field using the equation:

$$\sigma^{A(S)}_{xy} = \sigma_{xy}(H) - (+)\sigma_{xy}(-H) \quad (4)$$

The electrical measurements were performed in a ⁴He cryostat, capable of temperatures between 1.6 K – 360 K and magnetic fields up to 12 Teslas. Thermal stabilization was ensured during all measurements, monitored by a Cernox sensor element with a variation of less than 0.03% throughout the measurements. The tendency lines were calculated based on b-splines, and the dispersion across five different devices was used to calculate the errors.

Crystalline and epitaxial-quality determination

X-ray measurements were carried out on the thin film samples before and after the etching process using a four-circle Bruker D8 Discover thin film diffractometer. $\theta/2\theta$ measurements (Figure S1.a) were used to evaluate the highly oriented Ti-doped hematite films without any impurity phase present. Phi-scans (Figure S1.c) on the $(10\bar{1}4)$ peak allowed us to identify the orientations of the $[10\bar{1}0]$ planes. Figure S1.a shows the XRD pattern, where a diffraction peak at $2\theta = 39^\circ$ is observed, slightly smaller than the bulk value [39]. This confirms previous reports on homogeneous doping of hematite grown by PLD [40]. The absence of impurity phases and the (0001)-orientation of the films were further confirmed by $2\theta = \omega$ measurements (inset in Figure S1.a). The lattice parameters were calculated from the peak positions and found to reproduce the literature values of values of $a = 5.05(1) \text{ \AA}$ and $c = 13.72(2) \text{ \AA}$ [41]. Additionally, a ϕ scan (Figure S1.c) allows us to determine the in-plane orientation of the samples, which was used to pattern Hall bars in different orientations with respect to the crystallographic direction **a**.

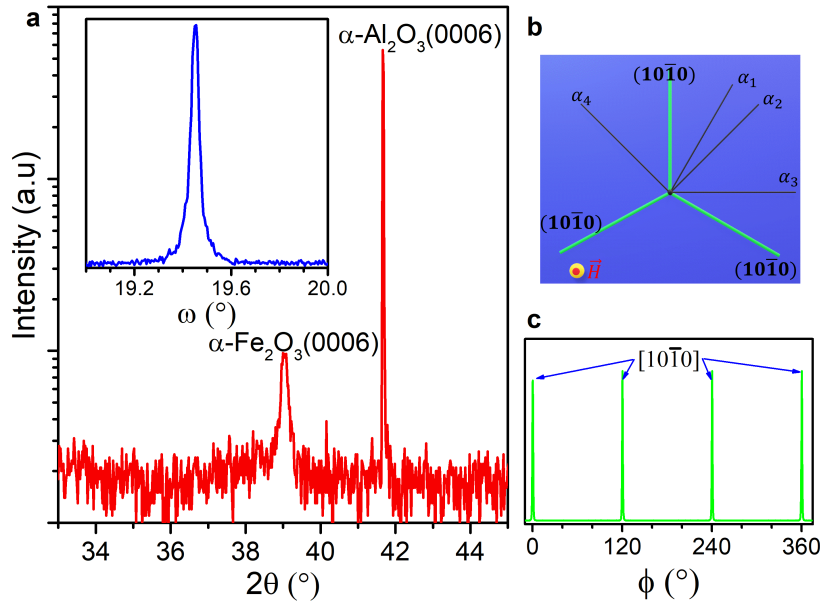


Figure S1: (a) The X-ray diffraction analysis of Ti-doped $\alpha\text{-Fe}_2\text{O}_3$ with (0001) orientation did not reveal any secondary phases. An inset of the film's (0006) peak showed that the films were epitaxial in nature. (b) The diagram illustrates the crystallographic plane's 3-fold symmetry, where α_2 and α_4 angles were equivalent with a field inversion, as were α_1 and α_3 . (c) The in-plane XRD scan further confirmed the crystal's symmetry, with a 120-degree separation and similar heights indicating a well-defined in-plane symmetry.

Magnetometry measurements

The SQUID measurements were performed using a commercial superconducting quantum interference device (SQUID) from Quantum Design. The films were saturated with 5 T at the starting temperature of 355 K, and then were cooled at a constant rate of 2 K/min under a static applied field of $\mu_0 H = 20$ mT. Due to the diamagnetic contribution

to the signal from the sapphire substrates used to grow the films and the mounting of the sample in the SQUID, a temperature-independent subtraction to the signal was made from the data from the average value of the magnetization below the observed transition for the temperature scans, and as a linear subtraction calculated at higher fields (± 3 T to ± 5 T) for the field scans. The Morin transition of the films was observed, characterized by a drop in magnetic moment to effectively zero above the background substrate contributions. The transition occurred at around 330 K, and at 320 K, the transition was complete, indicating that the films were in the purely easy-axis phase. The SQUID measurements agreed with other reports, where dopants were found to increase the Morin transition temperature even above room temperature [13]. The presence of Ti atoms did not significantly affect the magnetic moments in the samples, as the magnitude of the canted moment in the WFM phase fell within the range reported for pure single crystals [4, 39]. Both the temperature increment and the broadening of the Morin transition can be attributed to the smaller unit cell of the film as compared to the bulk values, leading to a change in the temperature dependence of the competing anisotropies that underlie the physics of the Morin transition[42]. We also note a soft loop at low magnetic fields in the easy-axis phase, possibly due to a thin ferrimagnetic seed layer that nucleates at the hematite/substrate interface [13, 43]

Transport properties on the weak ferromagnetic phase

The Hall conductivity also shows a dependence on the relative crystal orientation in the weak ferromagnetic phase, also showing a change of sign between different orientations of the Hall bar. Those aspects do not appear at lower fields on the EA phase and are not only contributions from the canted moment.

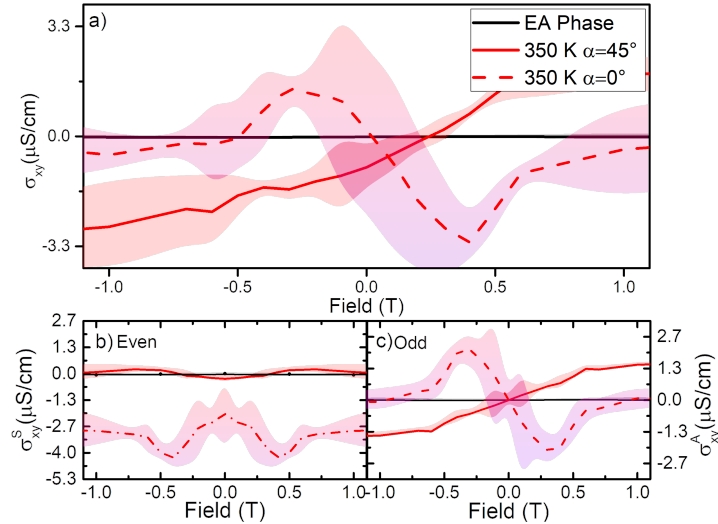


Figure S2: (a) Hall conductivity of devices along the easy-axis phase (**a**-axis) was measured and compared with the conductivity in the WFM phase and at a 45-degree relative orientation. The even (b) and odd (c) parts of the signal reveal a sign inversion in the odd contribution with the two relative orientations.

References

- [1] V. Baltz et al. “Antiferromagnetic spintronics”. In: *Rev. Mod. Phys.* 90 (1 Feb. 2018), p. 015005. DOI: 10.1103/RevModPhys.90.015005. URL: <https://link.aps.org/doi/10.1103/RevModPhys.90.015005>.
- [2] W. R. W. Ahmad et al. “A review on hematite α -Fe₂O₃ focusing on nanostructures, synthesis methods and applications”. In: *2016 IEEE Student Conference on Research and Development (SCORED)*. Dec. 2016, pp. 1–6. DOI: 10.1109/SCORED.2016.7810090.
- [3] A. Mirzaei, B. Hashemi, and K. Janghorban. “ α -Fe₂O₃ based nanomaterials as gas sensors”. In: *J. Mater. Sci. Mater. Electron.* 27.4 (Dec. 2015), 3109–3144. DOI: 10.1007/s10854-015-4200-z.
- [4] R. Lebrun et al. “Tunable long-distance spin transport in a crystalline antiferromagnetic iron oxide”. In: *Nature* 561.7722 (2018), 222–225. DOI: 10.1038/s41586-018-0490-7.
- [5] A. Ross et al. “Propagation Length of Antiferromagnetic Magnons Governed by Domain Configurations”. In: *Nano Lett.* 20.1 (Dec. 2020). PMID: 31809058, pp. 306–313. DOI: 10.1021/acs.nanolett.9b03837. eprint: <https://doi.org/10.1021/acs.nanolett.9b03837>. URL: <https://doi.org/10.1021/acs.nanolett.9b03837>.
- [6] A. Ross et al. “Structural sensitivity of the spin Hall magnetoresistance in antiferromagnetic thin films”. In: *Phys. Rev. B* 102 (9 Sept. 2020), p. 094415. DOI: 10.1103/PhysRevB.102.094415. URL: <https://link.aps.org/doi/10.1103/PhysRevB.102.094415>.
- [7] H. Meer et al. “Antiferromagnetic insulatronics: Spintronics in insulating 3d metal oxides with antiferromagnetic coupling”. In: *Appl. Phys. Lett.* 122.8 (Feb. 2023). 080502. ISSN: 0003-6951. DOI: 10.1063/5.0135079. eprint: https://pubs.aip.org/aip/apl/article-pdf/doi/10.1063/5.0135079/16715759/080502_1_online.pdf. URL: <https://doi.org/10.1063/5.0135079>.
- [8] Y. Cheng et al. “Electrical Switching of Tristate Antiferromagnetic Néel Order in α -Fe₂O₃ Epitaxial Films”. In: *Phys. Rev. Lett.* 124 (2 Jan. 2020), p. 027202. DOI: 10.1103/PhysRevLett.124.027202. URL: <https://link.aps.org/doi/10.1103/PhysRevLett.124.027202>.
- [9] E. Cogulu et al. “Direct imaging of electrical switching of antiferromagnetic Néel order in α -Fe₂O₃ epitaxial films”. In: *Phys. Rev. B* 103 (10 Mar. 2021), p. L100405. DOI: 10.1103/PhysRevB.103.L100405. URL: <https://link.aps.org/doi/10.1103/PhysRevB.103.L100405>.
- [10] F. J. Morin. “Magnetic Susceptibility of α -Fe₂O₃ and α -Fe₂O₃ with Added Titanium”. In: *Phys. Rev.* 78 (6 June 1950), pp. 819–820. DOI: 10.1103/PhysRev.78.819.2. URL: <https://link.aps.org/doi/10.1103/PhysRev.78.819.2>.
- [11] T. Dannegger et al. “Magnetic properties of hematite revealed by an ab initio parameterized spin model”. In: *Phys. Rev. B* 107 (18 May 2023), p. 184426. DOI: 10.1103/PhysRevB.107.184426. URL: <https://link.aps.org/doi/10.1103/PhysRevB.107.184426>.

- [12] G. A. Acket and J. Volger. “Electric transport in N-type Fe_2O_3 ”. In: *Physica* 32.9 (Sept. 1966), pp. 1543–1550. ISSN: 0031-8914. DOI: [https://doi.org/10.1016/0031-8914\(66\)90034-6](https://doi.org/10.1016/0031-8914(66)90034-6). URL: <https://www.sciencedirect.com/science/article/pii/0031891466900346>.
- [13] A. Ross et al. “An insulating doped antiferromagnet with low magnetic symmetry as a room temperature spin conduit”. In: *Appl. Phys. Lett.* 117.24 (Dec. 2020), p. 242405. DOI: 10.1063/5.0032940. eprint: <https://doi.org/10.1063/5.0032940>. URL: <https://doi.org/10.1063/5.0032940>.
- [14] J. Han et al. “Birefringence-like spin transport via linearly polarized antiferromagnetic magnons”. In: *Nat. Nanotechnol.* 15.7 (June 2020), 563–568. DOI: 10.1038/s41565-020-0703-8.
- [15] A. J. E. Rettie et al. “Synthesis, electronic transport and optical properties of $\text{Si}:\alpha\text{-Fe}_2\text{O}_3$ single crystals”. In: *J. Mater. Chem. C* 4 (3 Dec. 2016), pp. 559–567. DOI: 10.1039/C5TC03368C. URL: <http://dx.doi.org/10.1039/C5TC03368C>.
- [16] K.B. Vlasov et al. “Hall effect in hematite single crystals in the region of the Morin transition”. In: *Sov. Phys.-Solid State* 22 (May 1980), 967—969.
- [17] Sergey V. Ovsyannikov et al. “High-pressure cycling of hematite Fe_2O_3 : Nanostructuring, in situ electronic transport, and possible charge disproportionation”. In: *Phys. Rev. B* 86 (20 Nov. 2012), p. 205131. DOI: 10.1103/PhysRevB.86.205131. URL: <https://link.aps.org/doi/10.1103/PhysRevB.86.205131>.
- [18] B. Zhao et al. “Electrical transport properties of Ti-doped $\text{Fe}_2\text{O}_3(0001)$ epitaxial films”. In: *Phys. Rev. B* 84 (24 Dec. 2011), p. 245325. DOI: 10.1103/PhysRevB.84.245325. URL: <https://link.aps.org/doi/10.1103/PhysRevB.84.245325>.
- [19] J. Sinova et al. “Spin Hall effects”. In: *Rev. Mod. Phys.* 87 (4 Oct. 2015), pp. 1213–1260. DOI: 10.1103/RevModPhys.87.1213. URL: <https://link.aps.org/doi/10.1103/RevModPhys.87.1213>.
- [20] L. Wang et al. “Crystal-induced transverse current in collinear antiferromagnetic $\gamma\text{-FeMn}$ ”. In: *Appl. Phys. Lett.* 120.1 (Jan. 2022), p. 012403. DOI: 10.1063/5.0069504. eprint: <https://doi.org/10.1063/5.0069504>. URL: <https://doi.org/10.1063/5.0069504>.
- [21] J. Kipp et al. “The chiral Hall effect in canted ferromagnets and antiferromagnets”. In: *Commun. Phys.* 4.1 (May 2021). DOI: 10.1038/s42005-021-00587-3.
- [22] L. Šmejkal et al. “Crystal time-reversal symmetry breaking and spontaneous Hall effect in collinear antiferromagnets”. In: *Sci. Adv.* 6.23 (June 2020), eaaz8809. DOI: 10.1126/sciadv.aaz8809. eprint: <https://www.science.org/doi/pdf/10.1126/sciadv.aaz8809>. URL: <https://www.science.org/doi/abs/10.1126/sciadv.aaz8809>.
- [23] R. Shindou and N. Nagaosa. “Orbital Ferromagnetism and Anomalous Hall Effect in Antiferromagnets on the Distorted fcc Lattice”. In: *Phys. Rev. Lett.* 87 (11 Aug. 2001), p. 116801. DOI: 10.1103/PhysRevLett.87.116801. URL: <https://link.aps.org/doi/10.1103/PhysRevLett.87.116801>.
- [24] L. Šmejkal et al. “Topological antiferromagnetic spintronics”. In: *Nat. Phys.* 14.3 (Mar. 2018), 242–251. DOI: 10.1038/s41567-018-0064-5.

- [25] K. Samanta et al. “Crystal Hall and crystal magneto-optical effect in thin films of SrRuO₃”. In: *J. Appl. Phys.* 127.21 (June 2020), p. 213904. DOI: 10.1063/5.0005017. eprint: <https://doi.org/10.1063/5.0005017>. URL: <https://doi.org/10.1063/5.0005017>.
- [26] D.-F. Shao et al. “Interfacial Crystal Hall Effect Reversible by Ferroelectric Polarization”. In: *Phys. Rev. Appl.* 15 (2 Feb. 2021), p. 024057. DOI: 10.1103/PhysRevApplied.15.024057. URL: <https://link.aps.org/doi/10.1103/PhysRevApplied.15.024057>.
- [27] R.N. Bhowmik and A. G. Lone. “Electric field controlled magnetic exchange bias and magnetic state switching at room temperature in Ga-doped α -Fe₂O₃ oxide”. In: *J. Magn. Magn. Mater.* 462 (Sept. 2018), pp. 105–118. ISSN: 0304-8853. DOI: <https://doi.org/10.1016/j.jmmm.2018.05.007>. URL: <https://www.sciencedirect.com/science/article/pii/S0304885318306139>.
- [28] E. Gharibi et al. “ChemInform Abstract: Electrical Properties of Pure and Titanium-Doped Hematite Single Crystals, in the Basal Plane, at Low Oxygen Pressure.” In: *Chem. Inform.* 21.43 (Oct. 1990). DOI: <https://doi.org/10.1002/chin.199043022>. eprint: <https://onlinelibrary.wiley.com/doi/pdf/10.1002/chin.199043022>. URL: <https://onlinelibrary.wiley.com/doi/abs/10.1002/chin.199043022>.
- [29] , J. Sinova, and T. Jungwirth. “Beyond Conventional Ferromagnetism and Antiferromagnetism: A Phase with Nonrelativistic Spin and Crystal Rotation Symmetry”. In: *Phys. Rev. X* 12 (3 Sept. 2022), p. 031042. DOI: 10.1103/PhysRevX.12.031042. URL: <https://link.aps.org/doi/10.1103/PhysRevX.12.031042>.
- [30] T. R. Paudel et al. “Doping Rules and Doping Prototypes in A₂BO₄ Spinel Oxides”. In: *Advanced Functional Materials* 21.23 (3 Oct. 2011), pp. 4493–4501. DOI: <https://doi.org/10.1002/adfm.201101469>. eprint: <https://onlinelibrary.wiley.com/doi/pdf/10.1002/adfm.201101469>. URL: <https://onlinelibrary.wiley.com/doi/abs/10.1002/adfm.201101469>.
- [31] J. Robertson and S. J. Clark. “Limits to doping in oxides”. In: *Phys. Rev. B* 83 (7 Feb. 2011), p. 075205. DOI: 10.1103/PhysRevB.83.075205. URL: <https://link.aps.org/doi/10.1103/PhysRevB.83.075205>.
- [32] Y. L. Zhao et al. “Variable range hopping in TiO₂ insulating layers for oxide electronic devices”. In: *AIP Advances* 2.1 (3 Jan. 2012), p. 012129. ISSN: 2158-3226. DOI: 10.1063/1.3682346. eprint: https://pubs.aip.org/aip/adv/article-pdf/doi/10.1063/1.3682346/12876212/012129_1_online.pdf. URL: <https://doi.org/10.1063/1.3682346>.
- [33] S. Onoda, N. Sugimoto, and N. Nagaosa. “Quantum transport theory of anomalous electric, thermoelectric, and thermal Hall effects in ferromagnets”. In: *Phys. Rev. B* 77 (16 Apr. 2008), p. 165103. DOI: 10.1103/PhysRevB.77.165103. URL: <https://link.aps.org/doi/10.1103/PhysRevB.77.165103>.
- [34] P. J. Besser, A. H. Morrish, and C. W. Searle. “Magnetocrystalline Anisotropy of Pure and Doped Hematite”. In: *Phys. Rev.* 153 (2 Jan. 1967), pp. 632–640. DOI: 10.1103/PhysRev.153.632. URL: <https://link.aps.org/doi/10.1103/PhysRev.153.632>.
- [35] S. Foner. “High-Field Antiferromagnetic Resonance in Cr₂O₃”. In: *Phys. Rev.* 130 (1 Apr. 1963), pp. 183–197. DOI: 10.1103/PhysRev.130.183. URL: <https://link.aps.org/doi/10.1103/PhysRev.130.183>.

- [36] H. Meer et al. “Strain-induced shape anisotropy in antiferromagnetic structures”. In: *Phys. Rev. B* 106 (9 Sept. 2022), p. 094430. DOI: 10.1103/PhysRevB.106.094430. URL: <https://link.aps.org/doi/10.1103/PhysRevB.106.094430>.
- [37] D. A. Grave et al. “Heteroepitaxial hematite photoanodes as a model system for solar water splitting”. In: *J. Mater. Chem. A* 4 (8 Dec. 2016), pp. 3052–3060. DOI: 10.1039/C5TA07094E. URL: <http://dx.doi.org/10.1039/C5TA07094E>.
- [38] D. S. Perloff. “Four-point sheet resistance correction factors for thin rectangular samples”. In: *Solid State Electron.* 20 (3 Aug. 1977), pp. 681–687. DOI: 10.1103/PhysRevX.12.031042. URL: <https://link.aps.org/doi/10.1103/PhysRevX.12.031042>.
- [39] A.H. Morrish. *Canted Antiferromagnetism: Hematite*. Vol. 12. World Scientific, Jan. 1994, p. 031042. ISBN: 9789810220075. DOI: 10.1103/PhysRevX.12.031042. URL: <https://books.google.de/books?id=E2X8uW8UxmEC>.
- [40] K. D. Malviya et al. “Systematic comparison of different dopants in thin film hematite (α -Fe₂O₃) photoanodes for solar water splitting”. In: *J. Mater. Chem. A* 4 (8 Dec. 2016), pp. 3091–3099. DOI: 10.1039/C5TA07095C. URL: <http://dx.doi.org/10.1039/C5TA07095C>.
- [41] O. M. Lemine et al. “Rietveld analysis and Mössbauer spectroscopy studies of nanocrystalline hematite α -Fe₂O₃”. In: *J. Alloys Compd.* 502.2 (3 July 2010), pp. 279–282. ISSN: 0925-8388. DOI: <https://doi.org/10.1016/j.jallcom.2010.04.175>. URL: <https://www.sciencedirect.com/science/article/pii/S092583881001042X>.
- [42] J. O. Artman, J. C. Murphy, and S. Foner. “Magnetic Anisotropy in Antiferromagnetic Corundum-Type Sesquioxides”. In: *Phys. Rev.* 138 (3A May 1965), A912–A917. DOI: 10.1103/PhysRev.138.A912. URL: <https://link.aps.org/doi/10.1103/PhysRev.138.A912>.
- [43] I. Dzyaloshinsky. “A thermodynamic theory of “weak” ferromagnetism of antiferromagnetics”. In: *J. Phys. Chem. Solids* 4.4 (3 Aug. 1958), pp. 241–255. ISSN: 0022-3697. DOI: [https://doi.org/10.1016/0022-3697\(58\)90076-3](https://doi.org/10.1016/0022-3697(58)90076-3). URL: <https://www.sciencedirect.com/science/article/pii/0022369758900763>.